RSC Advances

PAPER

View Article Online
View Journal | View Issue

Cite this: *RSC Adv.*, 2025, **15**, 16525

Nanobubbles in graphene oxide synthesis: investigation of structure and physicochemical properties with boosting of oxygen content and microporous surface area†

Konstantinos N. Maroulas,[a] Nick Vordos,[b] Athanasios C. Mitropoulos[a] and George Z. Kyzas *[a]

Received 4th April 2025
Accepted 10th May 2025

DOI: 10.1039/d5ra02336j

rsc.li/rsc-advances

The present work reports an innovative modification of graphene oxide (GO) using air nanobubbles (NBs). A comprehensive set of characterizations, including Raman spectroscopy, FTIR, XRD, SEM, porosimetry, and SAXS, confirmed the improved structural features and functional groups. A notable increase in the specific surface area to the value of 109.4 m^2 (2.5-fold) was achieved through incorporation of the NBs, along with the introduction of microporosity, which significantly improved ion diffusion kinetics relative to previous methodologies. FTIR analyses confirmed the rise in oxygenated functional groups, mostly C–O entities, which improved the surface reactivity of GO@NBs. XRD confirmed the increase in crystallinity as well as greater crystal size in GO@NBs, while SAXS confirmed the structural integrity as well as material porosity. Air NBs, therefore, impact the physicochemical properties of GO extensively and reveal significant opportunities for energy storage, catalysis, and remediation.

Introduction

Graphene oxide (GO), the two-dimensional oxidized derivative of graphene, comprises a hexagonal lattice of carbon molecules adorned with functional oxygen groups in the form of hydroxyl, epoxy, carbonyl, and carboxyl units.[1] Such groups destabilize the sp^2 network while endowing hydrophilic character.[2] Produced through controlled oxidation of graphite, GO is a an important functionally versatile material in its own right, having applications in energy storage, composites, catalysis, biomedicine, and electronics. The tunable surface chemistry, high specific surface area, and covalent/non-covalent functionalization of GO render it a nanotechnology pillar that closes the gap between the excellent intrinsic properties of graphene and processability.[3] Recent structural models, like the Lerf–Klinowski model, highlight the dynamic interaction of sp^3-oxidized domains and sp^2-conjugated regions, governing the electronic, mechanical, and chemical properties of GO.[4] For example, Guerrero-Contreras and Caballero-Briones demonstrated that despite maintaining constant stable oxygen-to-carbon (O/C) ratios (~0.2), variability in the distribution of functional groups determined by the synthesis conditions, affects electrical resistance, optical absorption, and exfoliation efficiency greatly.[5] Thereby stressing the need for exacting structural control. Nevertheless, the non-stoichiometric nature of GO and susceptibility to synthesis conditions render reproducibility difficult, and advanced precautions need to be taken to tailor its functionality.

The heterogeneity in structure of GO driven by defect density, distribution of functional groups, and oxidation level constitutes a challenge as well as opportunity. Though oxygen functionalities enhance hydrophilicity and chemical activity, over-oxidation lowers the π-conjugated network, compromising electrical conductivity and mechanical strength.[6] Performed *via* traditional routes such as Brodie's (fuming HNO_3/$KClO_3$) and Hummers' (H_2SO_4/$NaNO_3$/$KMnO_4$), GO is prone to produce layers with random defect distributions, residual impurities (*e.g.*, sulfate esters), and environmental toxicity *via* the release of toxic gases through NO_2 and ClO_2 emissions and acidic waste.[7] Recent advances, however, highlight the employment of green processes, such as Marcano's modified Hummers' process, which excludes $NaNO_3$, employs H_3PO_4/H_2SO_4 mixture to enhance interlayer expansion, and reduces structural defects by intermediate stabilization. This approach not only minimizes environmental footprint but also increases carboxyl group concentration, optimizing GO for biomedical applications with edge-selective functionalization. Meanwhile, research identifies that the kinetics of oxidation and the quality of precursor graphite are influential factors on uniformity of functional groups.[8] For example, pre-exfoliated graphite

[a]*Hephaestus Laboratory, School of Chemistry, Faculty of Sciences, Democritus University of Thrace, GR-65404 Kavala, Greece. E-mail: kyzas@chem.duth.gr*

[b]*Department of Physics, Democritus University of Thrace, 65404 Kavala, Greece*

† Electronic supplementary information (ESI) available. See DOI: https://doi.org/10.1039/d5ra02336j

precursors, like in Sun–Fugetsu's synthesis, produce near-quantitative levels with less defect density, where pre-treatment is a key factor in scalable synthesis.[9] Additionally, solvent selection during synthesis and dispersion, such as acetone or ethanol, critically impacts GO's morphology and electrical properties. Zaaba *et al.* demonstrated that ethanol promotes agglomeration and higher conductivity due to enhanced flake contact, while acetone yields well-dispersed GO with larger interlayer spacing (0.75 nm *vs.* 0.71 nm), underscoring the solvent's role in tailoring GO for specific applications.[10] Despite these developments, the balancing act of oxidation to preserve sp^2 domains for charge transport, along with the incorporation of functional groups for targeted applications remains a central challenge.

In the last decade, the synthesis of GO has focused more on sustainability, scalability, and structural fidelity. Contemporary iterations of Hummers' process, as Tour's protocol, utilize H_3PO_4 to stabilize intermediates in the production of GO with high carboxyl content and minimized defects.[11] Today's advances at monitoring oxidation processes in real-time, such as *in situ* Raman spectroscopy, and by utilizing environmentally sustainable synthesis methods, such as electrochemical and plasma-assisted exfoliation, provide ways for reducing structural imbalances. Yet, difficulties still exist to obtain uniform oxygen supply and output maximization without influencing quality norms.

Conventional modification processes often have trade-offs associated with scalability, yield, and environmental impacts. Within the last few years, introducing NBs has become one of the novel processes in the field of materials science, due to their unique interfacial behaviors, extended stability, and high surface reactivity. While the majority of studies achieve porosity in GO through composite materials (*e.g.*, polymers, nanoparticles) or post-synthesis treatments like chemical activation or plasma etching, this study suggests the addition of NBs to the synthesis process. The role of NBs is to create hierarchical microporous structures within GO sheets. This eliminates the need for additives and preserves GO's inherent properties while addressing the absence of control over pore distribution in conventional methods like Hummers' or Staudenmaier's.[12–15] For instance, earlier work using γ-irradiation for pore formation used toxic reagents and was not scalable, whereas nanobubble-assisted synthesis offers a greener, tunable alternative.[16] NBs are gas bubbles stabilized by interfacial forces whose addition affects structural defects and hierarchical pore networks.[17] The process utilizes nanobubble collapse or stabilization to create conductive microporous channels, resulting in GO with enhanced oxidation uniformity, scalability, and porosity for energy storage or catalysis.[16,18] The process alleviates shortcomings of conventional GO synthesis by combining Marcano's green protocol with pore engineering using nanobubbles, opening a new pathway to manipulating GO's physicochemical properties.

The NBs addition can be explained simply: (i) they could be employed to increase exfoliation efficiency and modulate oxidation kinetics;[19] (ii) NBs with high surface energy and cavitation upon collapse, create localized shear forces that are employed to separate graphite layers with reduced reliance on harsh chemical oxidation, reducing structural defects and carbon lattice integrity;[20] Meanwhile, the gas–liquid interfaces of NBs facilitate oxygen diffusion, leading to homogeneous oxidation and higher oxygen functional group density (*e.g.*, epoxy, hydroxyl groups). The latter (pore formation and improved chemical oxidation) enhances surface area, porosity, and uniform structure in GO.[21–23] These pores minimize steric hindrance and offer interconnected channels for ion diffusion, decreasing resistance to ion transfer. Also, the porous structure has more oxygen functional groups exposed, enhancing electrostatic interactions with ions.[24,25] (iii) this controlled exfoliation enables larger, thinner GO sheets with more uniform morphology, and (iv) NBs can control oxidation through the formation of reactive species, optimizing the distribution of oxygen-containing functional groups on GO's structure for improved dispersibility, electrical conductivity, or mechanical strength.[26]

Materials and reagents

All the materials were used as received. Graphite flakes (75% over 150 μm), sulfuric acid (98%), potassium permanganate (99%) and hydrogen peroxide (30%) were supplied from Merck (Darmstadt, Germany). Ultrapure water containing bulk NBs with air were generated by counterflow hydrodynamic cavitation, as reported elsewhere.[27]

Synthesis of GO@NBs and GO

GO@NBs was synthesized following Marcano *et al.* method.[28] H_2SO_4 was combined with H_3PO_4 in a 9 : 1 (v/v) ratio. The purpose of adding orthophosphoric acid is to assist the injection of the oxidation solution.[11] Then, graphite flakes were placed in the acid mixture, followed by the addition of $KMnO_4$ (1 : 6 wt. ratio) in small portions, causing a temperature shift of 40–50 °C. The mixture was heated to 50 °C in a temperature-controlled water bath and stirred for 12 hours. As the process progressed, the mixture transformed into a paste. After 12 hours, ultrapure water containing air@NBs was added and the system was let to stir for 30 minutes. Finally, 30 wt% H_2O_2 was poured in the mixture, shifting the color to bright yellow. H_2O_2

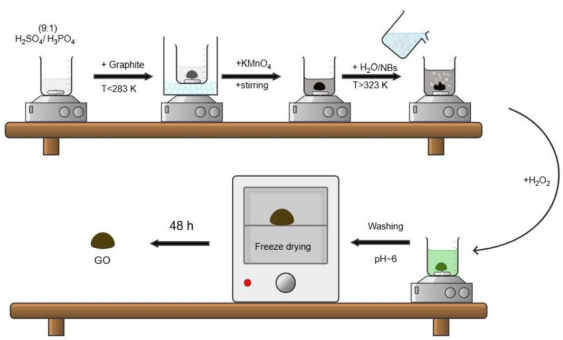

Fig. 1 Synthetic route of GO@NBs.

assisted the reduction of the manganese ion to soluble manganese sulphate and oxides. The produced GO washed with 200 mL HCl (37%), distilled water until pH ~ 6 and freeze-dried for 48 h. The synthetic route is presented in Fig. 1. GO was synthesized in the same way, using ultrapure water without NBs.

Results and discussion

SAXS was used as a structural characterization technique to analyze the architecture of the samples. As shown in Table S1† the comparison of radius of gyration (R_g) and fractal dimension (D_f) values, alongside the SAXS intensity profiles (Fig. 2), suggest that the higher of R_g value observed for GO@NB (20.95 nm) indicate larger, more extended structures, potentially reflecting well-dispersed graphene oxide sheets.[29,30] In contrast, the lower R_g value for GO (15.6 nm) suggest more compact, crumpled configurations. The fractal dimension values also indicate structural differences, with higher values ($D_f \sim 2.6$) for GO@NBs, suggesting a more complex surface structure or degree of aggregation, while lower values ($D_f \sim 1.8$) for GO point to less complex, more disordered or mass-like structures.[31,32]

The Kratky analysis supports these findings by indicating varying degrees of structural order among the samples. The Kratky curve of GO@NBs, indicate a more compact, folded structure, characteristic of well-organized GO sheets. According to the exponent (α), the higher value of GO@NBs ($\alpha = 1.6$) indicates a porous structure, while the lower value of GO ($\alpha = 0.3$) suggests smoother surfaces.[33,34] Overall, the combination of these analyses paints a picture of varying degrees of sheet dispersion, surface roughness, and aggregation, depending on the specific material treatment and composition.

XRD diffractograms of GO and GO@NBs are presented in Fig. 3. Both materials show the same peak at ~10.34°, which is the characteristic peak for GO, corresponding to the (001) lattice plane.[35] The *d*-spacing was calculated to be 0.86 nm based on Bragg's law.[36] Surprisingly GO@NBs showed much higher intensity (more than double) due to the presence of NBs. This led to a material with higher crystallinity and larger crystallite sizes, as shown in Table S2,† with fewer defects. The increment of crystallinity and crystal size in XRD data of GO@NBs is due to the structural reorganisation induced by NB. Shear forces induced by the collapse of NBs disrupt the restacking of graphene layers, creating hierarchical microporous networks while promoting localized ordering of smaller crystalline domains. This reduces lattice disorder and strain, leading to sharper XRD peaks and larger apparent crystal sizes determined by the Scherrer equation.[37–39] Furthermore, the homogeneity of functional group distribution could possibly improve due to the NBs' gas–liquid interfaces that enable oxygen diffusion upon oxidation. This reconciles sp^3 defect formation with intact sp^2 domains, favouring a more ordered yet porous structure.[40] The latter comes in full agreement with SAXS results.

Raman spectroscopy was utilized to examine the crystal structure, structural disorders, and defect structures in GO materials. The spectrums of GO and GO@NBs were measured

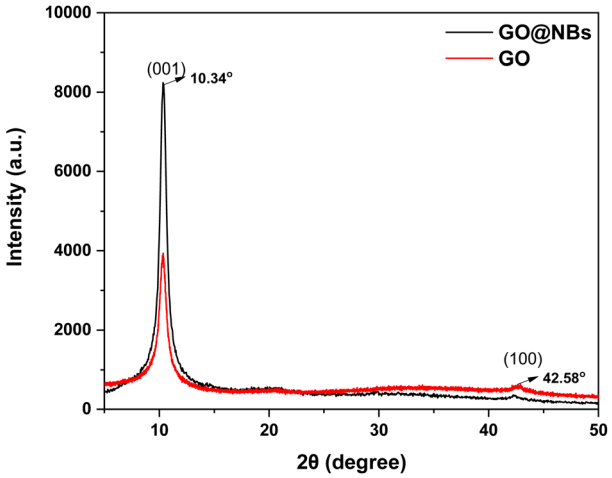

Fig. 3 XRD patterns of GO, GO@NBs.

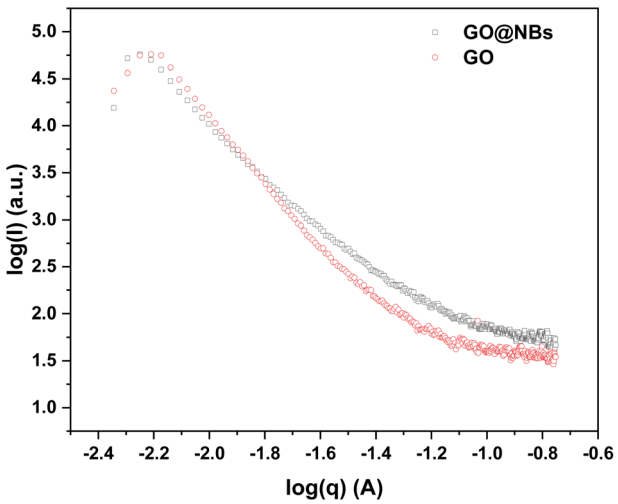

Fig. 2 SAXS profiles of GO, GO@NBs.

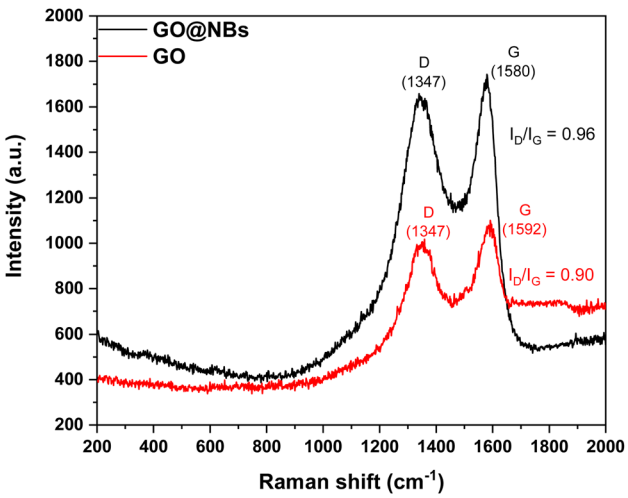

Fig. 4 Raman spectrum of GO, GO@NBs.

from 200 cm^{-1} to 2000 cm^{-1}, exhibiting the results presented in Fig. 4. The Raman G band is caused by the in-plane vibration of the C–C bond of the sp^2 orbital in crystalline graphite, whereas the D band is commonly referred to as the disordered band or defect band.[41] The latter is caused by the breathing motion of sp^2 atoms on the rings' edge planes, as well as graphite flaws. Both materials present D band at 1347 cm^{-1}, GO@NBs showed a G band at smaller wavenumbers (1580 cm^{-1}). This shift to lower values of G band indicates a higher oxidation degree for GO@NBs. This is in line with I_D/I_G, where GO@NBs exhibit a higher value concluding to a more disorder structure due to increased oxygen units. Both materials present I_D/I_G ratio ~1. The I_D/I_G ratio value is close to those reported in other papers with GO synthesis.[42,43]

The UV-vis spectrum of GO and GO@NBs is presented in Fig. 5. It shows a prominent peak at around 225–230 nm, attributable to the π–π* transition of the residual sp^2 C=C bonds and the extensive functionalization with oxygen groups. Furthermore, the faint shoulder at around 300 nm indicates the n–π* transition of the C=O bond.[44,45] GO@NBs seems to have a wider shoulder from 300–330 nm, indicating a higher degree of oxidation.

The improved synthesis with NBs further influences the number of functional units as can be seen in Fig. 6. Both materials exhibit the same peaks, which are commonly seen in GO. Specifically, they show a broad peak between 3500 and 3000 which is attributed to the O–H bond of hydroxyl and carboxyl units and a small peak at around 2200 which can be owed to alkyne groups.[46] Also, ketone (C=O) and epoxy (C–O) peaks can be seen in 1720 and 1050 cm^{-1}, respectively.[47]

In all cases GO@NBs exhibits broader peaks with higher intensity, leading to an increased number of oxygenated groups, compared to plain GO. The latter can be confirmed by comparing the ratio of the oxygenated groups (C=O, C–O, C–O–C).[48,49] As it can be observed in Table 1, GO@NBs have slightly increased ratio for C=O/C=C achieving a value of 1.12, compared to 0.92 of GO. However, biggest increase has been observed for C–O (hydroxyl and ether) and C–O–C (epoxy) units,

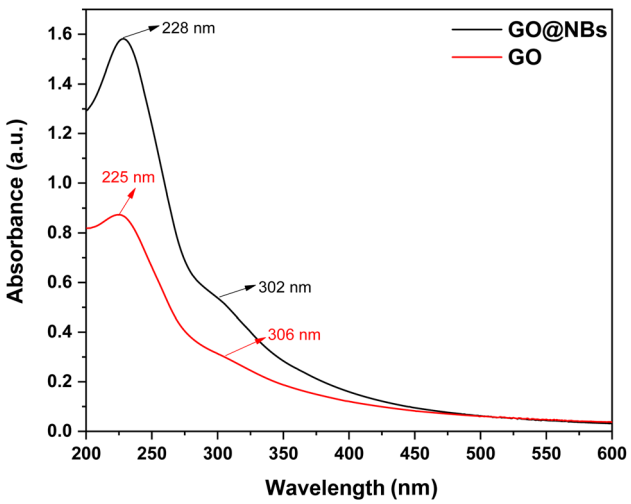

Fig. 5 UV-vis spectra of GO, GO@NBs.

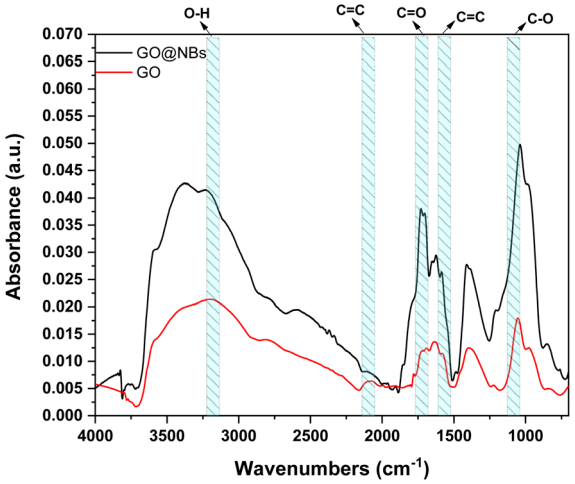

Fig. 6 FTIR spectra of GO, GO@NBs.

Table 1 Ratio of peak intensity of FTIR spectra of different oxygen groups to C=C

	GO	GO@NBs
C=O/C=C	0.92	1.12
C–O/C=C	1.05	2.19
C–O–C/C=C	0.90	1.50

where the values of the corresponding ratios has been almost doubled to 2.19 and 1.50, respectively. This is indicative of a higher oxidation degree, due to the incorporation of NBs in the synthesis steps.

The morphology of the materials can be seen in Fig. 7a for GO@NBs and Fig. 7b for GO. SEM images show that there are some morphological differences between the two GO samples. GO@NBs exhibit thin, crumpled sheet morphology under microscopy, indicative of exfoliation at the sheet level; however, SAXS and XRD analyses reveal a more compact and ordered structure overall, suggesting partial restacking or enhanced nanoscale ordering likely induced by interactions with NBs.[50] In contrast, GO appears to consist of larger, folded aggregates, which align with its lower SAXS fractal dimension and lower XRD crystallinity.[51] Also, GO@NBs have more dispersed, fragmental sheets compared to the denser interconnected network created by GO.[52] Thus, NBs inherited some structural differences in layer separation, sheet integrity, and surface homogeneity between these two materials.

The presence of NBs has influenced the physical characteristics of GO@NBs (Table 2). GO shows low BET surface area (44.22 $m^2\ g^{-1}$) with prevalence of mesopores (4.67 nm pore size) and very low microporosity (0.003 $cm^3\ g^{-1}$), GO@NBs records very high BET surface area (109.40 $m^2\ g^{-1}$) by forming a microporous structure (1.35 nm pore size) with six-fold enhancement of micropore volume (0.036 $cm^3\ g^{-1}$). This enhancement indicates that the synthesis changes effectively incorporated smaller pores, as attested to by the abrupt decrease in external surface area (26.09 $m^2\ g^{-1}$ compared to GO's 44.22 $m^2\ g^{-1}$), verifying that the higher BET area in GO@NBs is due to freshly developed

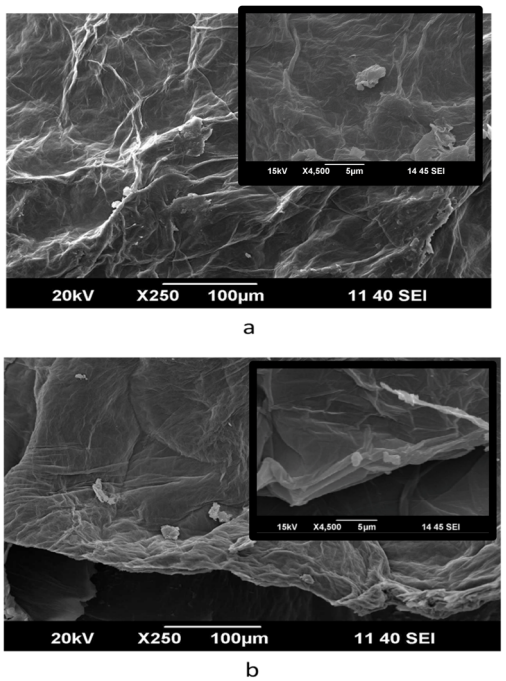

Fig. 7 SEM images of (a) GO@NBs and (b) GO (inset: higher magnification).

Table 2 Physical properties of GO, GO@NBs

Material	GO	GO@NBs
BET surface area (m^2 g^{-1})	44.22	109.40
External surface area (m^2 g^{-1})	44.22	26.09
DFT pore size (nm)	4.67	1.35
Cumulative pore volume (cm^3 g^{-1})	0.058	0.066
Micropore volume (cm^3 g^{-1})	0.003	0.036

micropores. The cumulative pore volume was also elevated (0.066 compared to 0.058 cm^3 g^{-1}), with a balance between micro- and mesoporosity. Generally, the synthesis enhancement in GO@NBs make it functionally better for the majority of high-surface-area applications.

Conclusions

In this study, we successfully improved the synthesis of GO by adding NBs in water. By doing so, we managed to increase significantly the specific surface area of GO@NBs by more than 2 times than GO, according to BET results. Also, XRD and SAXS results revealed that NBs improved the structural properties, while FTIR and Raman showed that NBs enhanced the oxidation efficiency and endowed more oxygenated groups to the material. Future research will optimize the GO's synthesis to further improve its properties.

Data availability

Data will be made available on request.

Author contributions

Konstantinos N. Maroulas: writing – review & editing, writing – original draft, methodology, investigation. Nick Vordos: writing – review & editing, writing – original draft, methodology, investigation. Athanasios C. Mitropoulos: conceptualization. George Z. Kyzas: writing – review & editing, writing – original draft, methodology, investigation, supervision.

Conflicts of interest

There are no conflicts to declare.

Acknowledgements

Authors thanks (i) Dr Kalliopi Ladomenou for taking the Raman spectrum and (ii) Dr Kosheleva Ramonna for taking the SEM images and N_2 porosimetry isotherm.

References

1 R. K. Singh, R. Kumar and D. P. Singh, Graphene oxide: strategies for synthesis, reduction and frontier applications, *RSC Adv.*, 2016, **6**, 64993–65011.
2 N. Yadav and B. Lochab, A comparative study of graphene oxide: hummers, intermediate and improved method, *FlatChem*, 2019, **13**, 40–49.
3 A. Adetayo and D. Runsewe, Synthesis and Fabrication of Graphene and Graphene Oxide: A Review, *Open J. Compos. Mater.*, 2019, **09**, 207–229.
4 V. Georgakilas, J. A. Perman, J. Tucek and R. Zboril, Broad Family of Carbon Nanoallotropes: Classification, Chemistry, and Applications of Fullerenes, Carbon Dots, Nanotubes, Graphene, Nanodiamonds, and Combined Superstructures, *Chem. Rev.*, 2015, **115**, 4744–4822.
5 J. Guerrero-Contreras and F. Caballero-Briones, Graphene oxide powders with different oxidation degree, prepared by synthesis variations of the Hummers method, *Mater. Chem. Phys.*, 2015, **153**, 209–220.
6 L. Sun, Structure and synthesis of graphene oxide, *Chin. J. Chem. Eng.*, 2019, **27**, 2251–2260.
7 A. Gutiérrez-Cruz, A. R. Ruiz-Hernández, J. F. Vega-Clemente, D. G. Luna-Gazcón and J. Campos-Delgado, A review of top-down and bottom-up synthesis methods for the production of graphene, graphene oxide and reduced graphene oxide, *J. Mater. Sci.*, 2022, **57**, 14543–14578.
8 F. Farjadian, S. Abbaspour, M. A. A. Sadatlu, S. Mirkiani, A. Ghasemi, M. Hoseini-Ghahfarokhi, N. Mozaffari, M. Karimi and M. R. Hamblin, Recent Developments in Graphene and Graphene Oxide: Properties, Synthesis, and Modifications: A Review, *ChemistrySelect*, 2020, **5**, 10200–10219.
9 L. Sun and B. Fugetsu, Mass production of graphene oxide from expanded graphite, *Mater. Lett.*, 2013, **109**, 207–210.
10 N. I. Zaaba, K. L. Foo, U. Hashim, S. J. Tan, W.-W. Liu and C. H. Voon, Synthesis of Graphene Oxide Using Modified

Hummers Method: Solvent Influence, *Procedia Eng.*, 2017, **184**, 469–477.
11 A. T. Habte and D. W. Ayele, Synthesis and Characterization of Reduced Graphene Oxide (rGO) Started from Graphene Oxide (GO) Using the Tour Method with Different Parameters, *Adv. Mater. Sci. Eng.*, 2019, **2019**, 5058163.
12 S. Sali, H. R. Mackey and A. A. Abdala, Effect of Graphene Oxide Synthesis Method on Properties and Performance of Polysulfone-Graphene Oxide Mixed Matrix Membranes, *Nanomaterials*, 2019, **9**, 769.
13 H. Bukovska, F. García-Perez, N. Brea Núñez, L. J. Bonales, A. Velasco, M. Á. Clavero, J. Martínez, A. J. Quejido, I. Rucandio and M. B. Gómez-Mancebo, Evaluation and Optimization of Tour Method for Synthesis of Graphite Oxide with High Specific Surface Area, *C*, 2023, **9**, 65.
14 Q. Zhang, Y. Yang, H. Fan, L. Feng, G. Wen and L.-C. Qin, Roles of water in the formation and preparation of graphene oxide, *RSC Adv.*, 2021, **11**, 15808–15816.
15 W. Du, H. Wu, H. Chen, G. Xu and C. Li, Graphene oxide in aqueous and nonaqueous media: dispersion behaviour and solution chemistry, *Carbon*, 2020, **158**, 568–579.
16 C. Yu, B. Zhang, F. Yan, J. Zhao, J. Li, L. Li and J. Li, Engineering nano-porous graphene oxide by hydroxyl radicals, *Carbon*, 2016, **105**, 291–296.
17 C. H. Y. Xuan Lim, A. Sorkin, Q. Bao, A. Li, K. Zhang, M. Nesladek and K. P. Loh, A hydrothermal anvil made of graphene nanobubbles on diamond, *Nat. Commun.*, 2013, **4**, 1556.
18 J. A. L. Willcox and H. J. Kim, Molecular Dynamics Study of Water Flow across Multiple Layers of Pristine, Oxidized, and Mixed Regions of Graphene Oxide, *ACS Nano*, 2017, **11**, 2187–2193.
19 Y. Weng, L. Li, S. Jiang, L. Qin and Y. Zhu, Nanobubble-assisted liquid phase exfoliation of graphene in deionized water, *Mater. Lett.*, 2024, **364**, 136372.
20 A. Verma, H. Paliwal and N. Gopinathan, A Classical Thermodynamic Model for Dispersed Nanophase Stability and Its Application for Investigating the Stability of Air Nanobubbles in Water, *Ind. Eng. Chem. Res.*, 2024, **63**, 18120–18133.
21 E. Iakovlev, P. Zhilyaev and I. Akhatov, Atomistic study of the solid state inside graphene nanobubbles, *Sci. Rep.*, 2017, **7**, 17906.
22 D. Shin, J. B. Park, Y.-J. Kim, S. J. Kim, J. H. Kang, B. Lee, S.-P. Cho, B. H. Hong and K. S. Novoselov, Growth dynamics and gas transport mechanism of nanobubbles in graphene liquid cells, *Nat. Commun.*, 2015, **6**, 6068.
23 F. Ma and D. Tao, A Study of Mechanisms of Nanobubble-Enhanced Flotation of Graphite, *Nanomaterials*, 2022, **12**, 3361.
24 M. Espanol, G. Mestres, T. Luxbacher, J.-B. Dory and M.-P. Ginebra, Impact of Porosity and Electrolyte Composition on the Surface Charge of Hydroxyapatite Biomaterials, *ACS Appl. Mater. Interfaces*, 2016, **8**, 908–917.
25 M. Zhang, K. Guan, Y. Ji, G. Liu, W. Jin and N. Xu, Controllable ion transport by surface-charged graphene oxide membrane, *Nat. Commun.*, 2019, **10**, 1253.
26 R. Ning, S. Yu, L. Li, S. A. Snyder, P. Li, Y. Liu, C. F. Togbah and N. Gao, Micro and nanobubbles-assisted advanced oxidation processes for water decontamination: the importance of interface reactions, *Water Res.*, 2024, **265**, 122295.
27 E. D. Michailidi, G. Bomis, A. Varoutoglou, G. Z. Kyzas, G. Mitrikas, A. C. Mitropoulos, E. K. Efthimiadou and E. P. Favvas, Bulk nanobubbles: production and investigation of their formation/stability mechanism, *J. Colloid Interface Sci.*, 2020, **564**, 371–380.
28 D. C. Marcano, D. V. Kosynkin, J. M. Berlin, A. Sinitskii, Z. Sun, A. Slesarev, L. B. Alemany, W. Lu and J. M. Tour, Improved Synthesis of Graphene Oxide, *ACS Nano*, 2010, **4**, 4806–4814.
29 S. N. H. Abbandanak, H. Aghamohammadi, E. Akbarzadeh, N. Shabani, R. Eslami-Farsani, M. Kangooie and M. H. Siadati, Morphological/SAXS/WAXS studies on the electrochemical synthesis of graphene nanoplatelets, *Ceram. Int.*, 2019, **45**, 20882–20890.
30 E. Chi, Y. Tang and Z. Wang, In Situ SAXS and WAXD Investigations of Polyamide 66/Reduced Graphene Oxide Nanocomposites during Uniaxial Deformation, *ACS Omega*, 2021, **6**, 11762–11771.
31 A. Y. Nugraheni, D. N. Jayanti, Kurniasari, S. Soontaranon, E. G. Rachman Putra and Darminto, Structural Analysis on Reduced Graphene Oxide Prepared from Old Coconut Shell by Synchrotron X-Ray Scattering, *IOP Conf. Ser.: Mater. Sci. Eng.*, 2017, **196**, 012007.
32 M. P. Weir, D. W. Johnson, S. C. Boothroyd, R. C. Savage, R. L. Thompson, S. R. Parnell, A. J. Parnell, S. M. King, S. E. Rogers, K. S. Coleman and N. Clarke, Extrinsic Wrinkling and Single Exfoliated Sheets of Graphene Oxide in Polymer Composites, *Chem. Mater.*, 2016, **28**, 1698–1704.
33 V. Singh Raghuwanshi, S. Varanasi, W. Batchelor and G. Garnier, Cellulose nanocrystals to modulate the self-assembly of graphene oxide in suspension, *Mater. Des.*, 2022, **216**, 110572.
34 R. Leite Rubim, M. Abrantes Barros, T. Missègue, K. Bougis, L. Navailles and F. Nallet, Highly confined stacks of graphene oxide sheets in water, *Eur. Phys. J. E*, 2018, **41**, 30.
35 K. N. Maroulas, A. Karakotsou, S. G. Poulopoulos, I. Konstantinou, K. Ladomenou and G. Z. Kyzas, Graphene adsorbents and photocatalysts derived from agricultural wastes: a review, *Sustainable Chemistry for the Environment*, 2024, **8**, 100166.
36 H. Cole, Bragg's law and energy sensitive detectors, *J. Appl. Crystallogr.*, 1970, **3**, 405–406.
37 X. Jiao, Y. Qiu, L. Zhang and X. Zhang, Comparison of the characteristic properties of reduced graphene oxides synthesized from natural graphites with different graphitization degrees, *RSC Adv.*, 2017, **7**, 52337–52344.
38 V. Gupta, N. Sharma, U. Singh, M. Arif and A. Singh, Higher oxidation level in graphene oxide, *Optik*, 2017, **143**, 115–124.
39 T. Taniguchi, L. Nurdiwijayanto, N. Sakai, K. Tsukagoshi, T. Sasaki, T. Tsugawa, M. Koinuma, K. Hatakeyama and S. Ida, Revisiting the two-dimensional structure and

reduction process of graphene oxide with in-plane X-ray diffraction, *Carbon*, 2023, **202**, 26–35.

40 L. Stobinski, B. Lesiak, A. Malolepszy, M. Mazurkiewicz, B. Mierzwa, J. Zemek, P. Jiricek and I. Bieloshapka, Graphene oxide and reduced graphene oxide studied by the XRD, TEM and electron spectroscopy methods, *J. Electron Spectrosc. Relat. Phenom.*, 2014, **195**, 145–154.

41 A. M. Dimiev and J. M. Tour, Mechanism of Graphene Oxide Formation, *ACS Nano*, 2014, **8**, 3060–3068.

42 N. Chadha, R. Sharma and P. Saini, A new insight into the structural modulation of graphene oxide upon chemical reduction probed by Raman spectroscopy and X-ray diffraction, *Carbon Lett.*, 2021, **31**, 1125–1131.

43 N. Sharma, V. Sharma, Y. Jain, M. Kumari, R. Gupta, S. K. Sharma and K. Sachdev, Synthesis and Characterization of Graphene Oxide (GO) and Reduced Graphene Oxide (rGO) for Gas Sensing Application, *Macromol. Symp.*, 2017, **376**, 1700006.

44 V. Gupta, N. Sharma, U. Singh, M. Arif and A. Singh, Higher oxidation level in graphene oxide, *Optik*, 2017, **143**, 115–124.

45 R. P. Reshma, N. S. Abishek and K. N. Gopalakrishna, Synthesis and characterization of graphene oxide, tin oxide, and reduced graphene oxide-tin oxide nanocomposites, *Inorg. Chem. Commun.*, 2024, **165**, 112451.

46 M. Namvari, L. Du and F. J. Stadler, Graphene oxide-based silsesquioxane-crosslinked networks – synthesis and rheological behavior, *RSC Adv.*, 2017, **7**, 21531–21540.

47 A. Koltsakidou, K. N. Maroulas, E. Evgenidou, D. N. Bikiaris, G. Z. Kyzas and D. A. Lambropoulou, Removal of the antidepressants bupropion and sertraline from aqueous solutions by using graphene oxide: a complete adsorption/desorption evaluation for single-component and binary mixtures, *J. Mol. Liq.*, 2025, **424**, 127147.

48 F. Han Lyn, T. Chin Peng, M. Z. Ruzniza and Z. A. Nur Hanani, Effect of oxidation degrees of graphene oxide (GO) on the structure and physical properties of chitosan/GO composite films, *Food Packag. Shelf Life*, 2019, **21**, 100373.

49 Khairuddin, E. Pramono, S. B. Utomo, V. Wulandari, A. Zahrotul W and F. Clegg, FTIR studies on the effect of concentration of polyethylene glycol on polymerization of Shellac, *J. Phys.: Conf. Ser.*, 2016, **776**, 012053.

50 M. M. Hulagabali, G. R. Vesmawala and Y. D. Patil, Synthesis, characterization, and application of graphene oxide and reduced graphene oxide and its influence on rheology, microstructure, and mechanical strength of cement paste, *Journal of Building Engineering*, 2023, **71**, 106586.

51 W. C. H. Silva, M. A. Zafar, S. Allende, M. V. Jacob and R. Tuladhar, Sustainable Synthesis of Graphene Oxide from Waste Sources: A Comprehensive Review of Methods and Applications, *Materials Circular Economy*, 2024, **6**, 23.

52 B. Anegbe, I. H. Ifijen, M. Maliki, I. E. Uwidia and A. I. Aigbodion, Graphene oxide synthesis and applications in emerging contaminant removal: a comprehensive review, *Environ. Sci. Eur.*, 2024, **36**, 15.